http://dx.doi.org/10.5012/bkcs.2012.33.9.2897

New Donor Materials Based on Thiazole and Triphenylamine for Photovoltaic Devices

Tak-kyun Ro and Jong-In Hong*

Department of Chemistry, College of Natural Sciences, Seoul National University, Seoul 151-747, Korea
**E-mail: jihong@snu.ac.kr*
Received April 13, 2012, Accepted May 26, 2012

New photovoltaic donor materials, 4,4'-(2,2'-bithiazole-5,5'-diyl)bis(*N,N*-diphenylbenzenamine) (**BDT**) and 4-(2,2'-bithiazol-5-yl)-*N,N*-diphenylbenzenamine (**BT**), were synthesized. A solution processable triphenylamine-containing bithiazole (**BDT** and **BT**) was blended with a [6,6]-phenyl C_{61} butyric acid methyl ester (PCBM) acceptor to study the performance of small-molecule-based bulk heterojunction (BHJ) photovoltaic devices. Optimum device performance was achieved after annealing, for device with a **BDT**/PCBM ratio of 1:4. The open-circuit voltage, short-circuit current, and power conversion efficiency of the device with the aforementioned **BDT**/PCBM ratio were 0.51 V, 4.10 mA cm^{-2}, and 0.68%, respectively, under simulated AM 1.5 solar irradiation (100 mW cm^{-2}).

Key Words : Thiazole, Organic photovoltaic cells, Bulk-heterojunction, Triphenylamine

Introduction

Because of the current energy problem, it has become necessary to develop new renewable energy sources. Organic photovoltaics (OPVs) are considered to be one of the most promising candidates for such new enery sources because of the following advantages: ease of synthesis, low cost, and ease of device fabrication.[1,2] To date, the most successful materials for OPVs are thiophene-based polymers blended with small molecules such as fullerene and [6,6]-phenyl C_{61} butyric acid methyl ester (PCBM).[3] Synthesis, purification, and energy level control are easier in the case of small molecules than in the case of polymers. Consequently, many research groups have focused on small-molecule OPVs in which thiophene derivatives are used as donor materials; this is because of the excellent charge-transport ability and high thermal stability of thiophene derivatives.[4] Furthermore, the feasibility of using triphenylamine (TPA) moiety in OPVs has been widely investigated because of its hole-transport and electron-donating ability, thermal and electrochemical stability, and isotropic optical and charge transport properties.[5-7]

Recently, Shirota, Roncali, and co-workers have developed TPA derivatives with propeller-shaped and three-dimensional (3-D) star-shaped molecules; the three phenyl groups in these derivatives are not in the same plane.[5,6] In addition, Li and co-workers synthesized star-shaped organic molecules linked with electron-rich TPA units and electron-poor benzothiadiazole units.[8] They designed very high performance organic solar cells (OSC) by using these solution-processable organic molecules.[8d] Various electron-poor moieties such as benzothiadiazole,[9] thienopyrazine,[10] and thiazole[11] units have been used in organic photovoltaics.

In our previous study,[12] we synthesized solution-processable and thermally stable donor materials comprising a bithiophene unit and a TPA unit linked by conjugated bonds for bulk heterojunction photovoltaics. The device with the best performance showed a power conversion efficiency (PCE) of 0.34% under simulated AM 1.5 solar irradiation at 100 mW cm^{-2}. The low PCE was due to the poor morphology of the blended solid film of the donor material and PCBM. Herein, we report the design of new donor materials, 4,4'-(2,2'-bithiazole-5,5'-diyl)bis(*N,N*-diphenylbenzenamine) (**BDT**) and 4-(2,2'-bithiazol-5-yl)-*N,N*-diphenylbenzenamine (**BT**), consisting of a TPA unit and thiazole unit linked by conjugated bonds. We successfully used these donor materials for the fabrication of BHJ OPV devices (Fig. 1). The PCEs of the OPV devices fabricated using **BDT** and **BT** were better than those of the devices fabricated using thiophene derivatives[12] because of the better morphology of the solid film obtained by blending **BDT** and PCBM. Optimum device performance was achieved for a **BDT**/PCBM ratio of 1:4, after annealing; the open-circuit voltage (V_{oc}), short-circuit current (J_{sc}), and PCE of the device with the aforementioned **BDT**/PCBM ratio were 0.51 V, 4.10 mA cm^{-2}, and 0.68%, respectively, under simulated AM 1.5 solar irradiation (100 mW cm^{-2}).

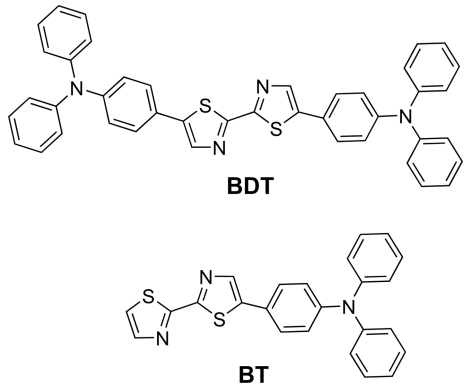

Figure 1. Molecular structures of **BDT** and **BT**.

Experimental

Materials and Instrument. 4-(Diphenylamino)phenylboronic acid, tetrakis(triphenyl-phospine)palladium(0) ($Pd(PPh_3)_4$), PCBM, and 2,9-dimethyl-4,7-diphenyl-1,10-phenanthroline (BCP) were purchased from Aldrich and LMC. Poly(3,4-ethylenedioxythiophene)-poly(styrenesulfonate) (PEDOT:PSS) was purchased from Baytron. 5,5'-Dibromo-2,2'-bithiazole **1** and 5-bromo-2,2'-bithiazole **2** were synthesized according to previously reported the procedures.[13] Analytical thin-layer chromatography was performed using Kieselgel 60F-254 plates from Merck. Column chromatography was carried out on Merck silica gel 60 (70-230 mesh). All the solvents and reagents were commercially available and used without further purification, unless otherwise noted. ^{1}H and ^{13}C NMR spectra were recorded in $CDCl_3$ by using an Advance 300 or 500 MHz Bruker spectrometer. The ^{1}H NMR chemical shifts in $CDCl_3$ were referenced to $CHCl_3$ (7.27 ppm), and the ^{13}C NMR chemical shifts in $CDCl_3$ are reported relative to $CHCl_3$ (77 ppm). UV-vis spectra were recorded using a Beckman DU 650 spectrophotometer. High-resolution mass spectra were obtained using a Bruker MALDI-TOF mass spectrometer. Fluorescence spectra were recorded using a Jasco FP-7500 spectrophotometer. Cyclic voltammetry (CV) was performed using a CH instruments 660 electrochemical analyzer. AFM images of spin-coated thin films were obtained using a PSIA XE-150 advanced scanning microscope.

Synthesis.

4,4'-(2,2'-Bithiazole-5,5'-diyl)bis(*N*,*N*-diphenylbenzenamine) (BDT): A mixture of **1** (200 mg, 0.61 mmol), 4-(diphenylamino)phenylboronic acid (444 mg, 1.53 mmol), tetrakis-(triphenylphospine)-palladium(0) (71 mg, 0.06 mmol), and potassium carbonate (340 mg, 2.45 mmol) in THF/H_2O (30 mL) was refluxed for 24 h. After cooling to room temperature, the solvent was evaporated under vacuum, and the reaction mixture was extracted with dichloromethane. The organic phase was washed with water and dried over Na_2SO_4. The solvent was evaporated to give a reddish product. This crude product was purified by silica gel column chromatography using ethyl acetate-hexane as the eluent and recrystallized from a mixture of dichloromethane and hexane to obtain a reddish solid product (yield: 390 mg, 97%). ^{1}H NMR (300 MHz, $CDCl_3$) δ 7.97 (s, 2H), 7.49 (d, 9 Hz, 4H), 7.31 (m, 15 Hz, 8H), 7.12 (m, 30 Hz, 16H). ^{13}C NMR (125 MHz, $CDCl_3$) δ 159.5, 148.7, 147.3, 141.5, 138.7, 129.7, 127.8, 125.2, 124.4, 123.9, 123.2. Mass: calcd. for $C_{42}H_{31}N_4S_2$ $[M+H]^+$ 655.1990, HR-Mass: $[M+H]^+$ 655.1996.

4-(2,2'-Bithiazol-5-yl)-*N*,*N*-diphenylbenzenamine (BT): A mixture of **2** (150 mg, 0.61 mmol), 4-(diphenylamino)-phenylboronic acid (211 mg, 0.73 mmol), tetrakis(triphenylphospine)palladium(0) (35 mg, 0.03 mmol), and potassium carbonate (168 mg, 1.21 mmol) in THF (15 mL) and H_2O (1.5 mL) was refluxed for 24 h. After cooling to room temperature, the solvent was evaporated under vacuum, and the reaction mixture was extracted with dichloromethane. The organic phase was washed with water and dried over Na_2SO_4. The solvent was evaporated to give an orange-reddish product; the crude product was purified by silica gel column chromatography using ethyl acetate-hexane as the eluent and recrystallized from dichloromethane and hexane to afford an orange-red solid (yield: 240 mg, 96%). ^{1}H NMR (300 MHz, $CDCl_3$) δ 7.97 (s, 1H), 7.92 (d, 3 Hz, 1H), 7.47 (m, 18 Hz, 3H), 7.32 (m, 15 Hz, 3H), 7.12 (m, 10 Hz, 9H). ^{13}C NMR (125 MHz, $CDCl_3$) δ 162.1, 159.3, 148.8, 147.3, 144.1, 141.8, 138.6, 129.7, 127.8, 125.2, 124.2, 123.9, 123.1, 120.8. Mass: calcd. for $C_{24}H_{17}N_3S_2$ $[M]^+$ 411.0864, HR-Mass: 411.0870.

OSCs Fabrication. OPVs with the traditional structure were fabricated with an ITO anode and metal cathode. The ITO glass was cleaned in an ultrasonic bath containing acetone and isopropanol. Then, a thin layer (30 nm) of PEDOT:PSS was spin-coated on the ITO glass. Next, the active layer was prepared by spin-coating a blend of **BDT** or **BT** and PCBM at different weight ratios (1:3 to 1:5) onto the PEDOT:PSS layer (*ca.* 45 nm thickness). Subsequently, an exciton-blocking layer (EBL) of BCP (10 nm) was deposited on the active layer under vacuum (10^{-4} Pa). Finally, an Al metal electrode layer (100 nm) was vacuum-deposited on the BCP layer. We measured the device performance before and after annealing at 80 °C for 20 min in a nitrogen glove box. Current-voltage (*J*–*V*) measurements for the devices were performed using a Keithley 237 instrument. The device performances were characterized under uniform illumination (AM 1.5 G illumination intensity of 100 mW cm^{-2}) using a solar simulator. The light intensity at each wavelength was calibrated using a standard Si solar cell as a reference.

Electrochemical Characterization. Cyclic voltammetry (CV) experiments were performed to measure the electrochemical properties of **BDT** and **BT** in CH_2Cl_2. In the CV experiments, a glassy carbon electrode, a platinum wire, and 0.1 M tetra-*n*-butylammonium hexafluorophosphate ($TBAPF_6$) were used as the working electrode, counter electrode, and supporting electrolyte, respectively. $Ag/AgNO_3$ was used as the reference electrode (at room temperature) and calibrated against a standard hydrogen electrode (SHE) using ferrocene/ferrocenium (Fc/Fc^+).

Results and Discussion

BDT and **BT** were synthesized by a Suzuki coupling reaction between 5,5'-dibromo-2,2'-bithiazole or 5-bromo-2,2'-bithiazole[13] and 4-(diphenylamino)phenylboronic acid, respectively (Scheme 1).

The absorption and emission spectra of **BDT** and **BT** in CH_2Cl_2, quartz solid film, and films composed of a **BDT** (or **BT**)/PCBM blend are shown in Figure 2 and S1†. Table 1 lists the main photophysical and electrochemical properties of **BDT** and **BT**.

The UV-Vis spectra in CH_2Cl_2 solution showed two absorption bands with maxima at 300 and 437 nm for **BDT** and at 300 and 399 nm for **BT**. The absorption peak at 300 nm was due to the triphenylamine unit, and the peaks at 437

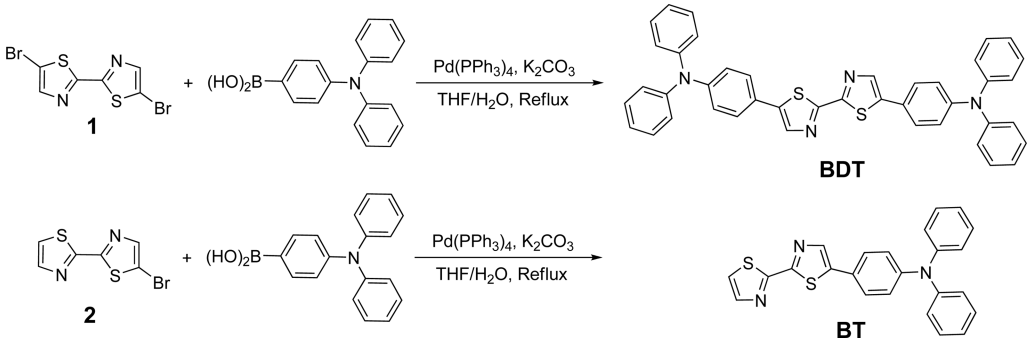

Scheme 1. Synthesis of **BDT** and **BT**.

and 399 nm were due to the bithiazole unit. The absorption spectra in quartz solid film showed maxima at 306 and 442 nm for **BDT** and at 307 and 412 nm for **BT**. The emission spectra in CH_2Cl_2 solution showed maxima at 544 nm and 530 nm for **BDT** and **BT**, respectively. In the quartz solid film, the emission spectra showed a maximum at 552 nm for **BDT** and at 545 nm for **BT**. The emission spectra of **BDT** and **BT** in the quartz solid film were red-shifted with respect to those in CH_2Cl_2 solution by approximately 8 and 15 nm, respectively, because of self-aggregation and intermolecular interactions. The UV-vis absorption and PL emission of **BDT** were red-shifted with respect to those of **BT** owing to the longer conjugation length of **BDT**. The emission spectra of the **BDT**/PCBM and **BT**/PCBM blend films were drastically quenched by PCBM (Fig. 2(b)). This phenomenon indicates energy transfer from the excited states of **BDT** and **BT** to PCBM and intermolecular photoinduced charge transfer (PICT).[7,14] **BDT** and **BT** were used as the electron donor materials, and PCBM was used as the electron acceptor material in the **BDT**/PCBM and **BT**/PCBM blended films. This PICT process also ocurrs in the case of a conducting conjugated polymer and PCBM blend.[14]

The cyclic voltammograms of **BDT** and **BT** revealed a reversible oxidation process (Fig. 3). The oxidation potential energies of **BDT** and **BT** were measured to be $E_{1/2,ox}$ = 0.69 and 0.70 V *vs.* Ag/Ag^+, respectively. The HOMO energy levels of **BDT** (−5.01 eV) and **BT** (−5.02 eV) were calculated from $E_{1/2,ox}$ after correction for the vacuum energy level (4.50 eV) (Table 1). The LUMO energy levels of **BDT** (−2.51 eV) and **BT** (−2.31 eV) were calculated from the cross-sectional wavelength between the absorption and emission spectra (Table 1). The electrochemical bandgap of **BDT** was slightly narrower than that of **BT** because of the difference in the conjugation lengths of **BDT** and **BT**; this difference in the conjugation length was in turn due to the difference in the number of TPA units in these two donors.

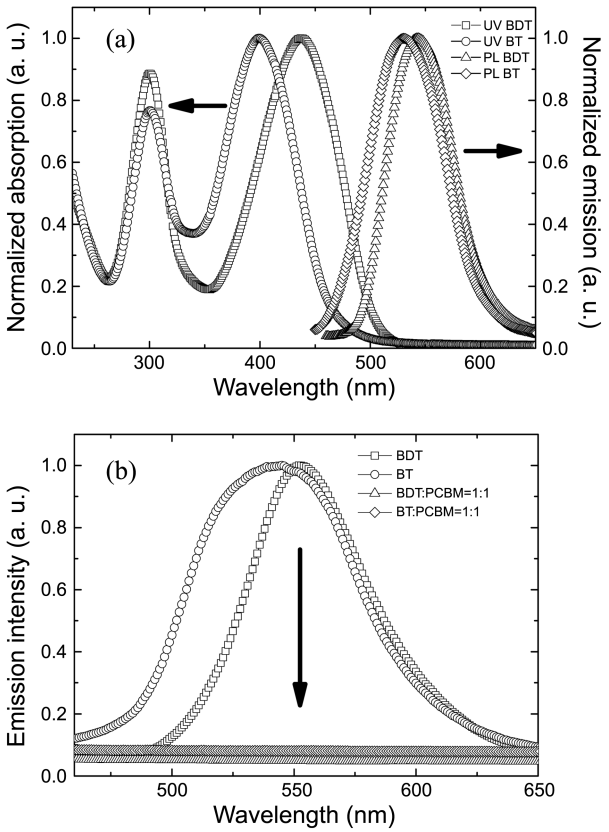

Figure 2. UV and PL spectra of **BDT** and **BT** in CH_2Cl_2 (a), **BDT** and **BT** neat solid film (b) and the films containing blend of **BDT** or **BT** and PCBM at 1:1 ratios (b).

Table 1. Photophysical and electrochemical properties of **BDT** and **BT**

	Absorption (λ_{nm}) (ε/M cm)[a]	Emission (λ_{nm})[a]	HOMO[b] (eV)	LUMO[c] (eV)	ΔE[d] (eV)
BDT	300(60140), 437(67855) (solution) 306, 442 (film)	544 (solution) 552 (film)	−5.01	−2.51	2.50
BT	300(21085), 399(27505) (solution) 307, 412 (film)	530 (solution) 545 (film)	−5.02	−2.31	2.71

[a]Absorption and emission spectra were measured in 0.02 mM CH_2Cl_2 solution and quartz solid film. [b]HOMO energy levels were determined in CH_2Cl_2 solution (0.1 M $TBAPF_6$) *vs.* $AgNO_3$. HOMO = $E_{1/2,ox}$ + 4.50 eV. [c]LUMO energy levels were calculated from the cross sectional wavelength between absorption and emission spectra. [d]ΔE = HOMO-LUMO.

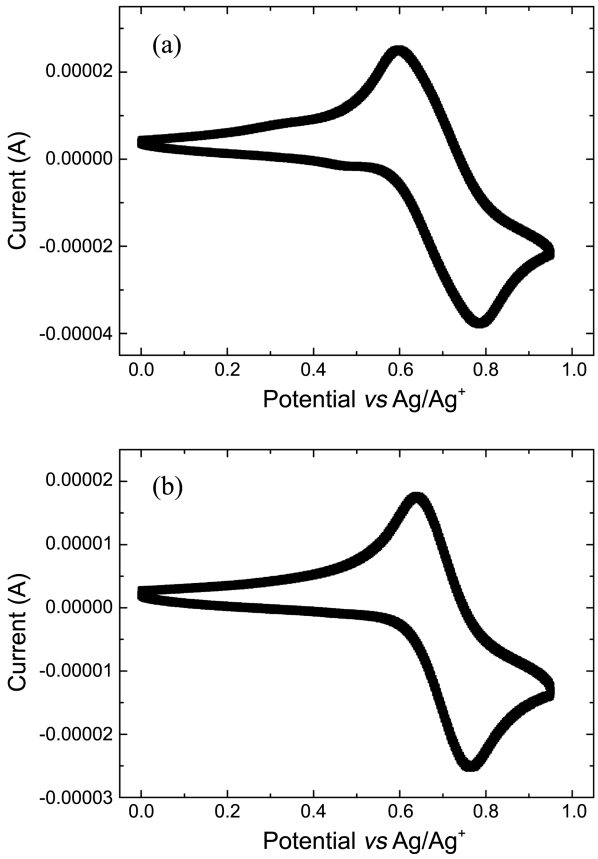

Figure 3. Cyclic voltammograms of 1.0 mM **BDT** (a) and **BT** (b) in CH_2Cl_2 solution. Scan rate is 0.2 Vs^{-1}.

To examine the photovoltaic performances, bulk heterojunction solar cell devices were fabricated with a sandwich structure: ITO/PEDOT:PSS (30 nm)/**BDT** or **BT**:PCBM (45 nm)/BCP (10 nm)/Al (100 nm). The *J-V* performances of the devices are shown in Figure 4 and S2†, and summarized in Table 2. In order to optimize the device properties, different **BDT** or **BT** and PCBM ratios were employed. In a case where **BDT**/PCBM or **BT**/PCBM = 1:3, the power conversion efficiencies of the devices were 0.15% and 0.018%, respectively. As the PCBM concentration increased, in the case of **BDT**/PCBM or **BT**/PCBM = 1:4, the power conversion efficiencies of the devices increased by *ca.* 4 times and 10 times, to 0.53% and 0.17%, respectively. Similarly, in the case of **BDT**/PCBM or **BT**/PCBM = 1:5, the power conversion efficiencies of the devices were 0.56% and 0.44%, respectively. As a result, for both **BDT** and **BT**, by increasing the PCBM concentration from 1:3 to 1:5, the power conversion efficiencies of the devices were improved due to efficient PICT to PCBM. Since the extinction coefficient of **BDT** is larger than **BT**, the power conversion efficiency of the **BDT**/PCBM blended devices was better than that of the **BT**/PCBM blended devices.

Figure 4 shows the *J-V* curves of bulk heterojunction devices before and after annealing. In the case of **BDT**/PCBM or **BT**/PCBM = 1:3 after annealing, the power conversion efficiencies of the devices increased by *ca.* four times and two times to 0.54% and 0.031%, respectively.

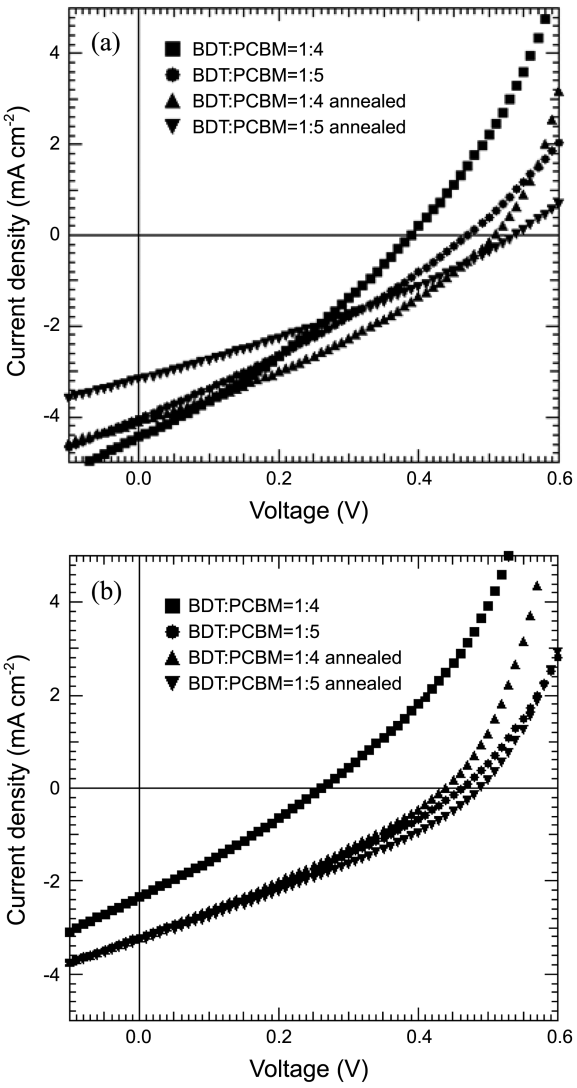

Figure 4. *J-V* curves of devices based on **BDT** (a) or **BT** (b) and PCBM at different weight ratios (1:4, 1:5) before and after annealing under simulated AM 1.5 solar irradiation at 100 mW cm^{-2}.

After the annealing of **BDT**/PCBM or **BT**/PCBM = 1:4, the power conversion efficiencies of the devices were slightly increased to 0.68% and 0.42%, respectively. Similarly, in the case of **BT**/PCBM = 1:5, the power conversion efficiency of the device was 0.49%. Consequently, in all cases of **BDT**/PCBM or **BT**/PCBM, the open-circuit voltage, short-circuit current, and fill factor of the devices increased after annealing, with two exceptions (**BDT**/PCBM = 1:4 and 1:5). The overall device data based on **BDT** or **BT** are summarized in Table 2.

In order to explain the difference in the PCEs of the devices, atomic force microscopy (AFM) was employed to examine the film morphologies of the blended films.[15,16] The AFM images of the devices are shown in Figure 5 and S3†. The surface of the blended film with a **BDT**/PCBM ratio of 1:3 had a surface with a root-mean-square (rms) roughness of 0.13 nm; the film with a **BDT**/PCBM ratio of 1:4 had an rms roughness of 0.19 nm. Similarly, the rms roughnesses of

Table 2. Device performance of bulk heterojunction solar cell based on **BDT** or **BT** and PCBM with different ratios (1:3 to 1:5) and annealing under simulated AM 1.5 solar irradiation at 100 mWcm^{-2}

Active layer		V_{OC} (V)		J_{SC} (mA cm^{-2})		FF (%)		PCE (%)	
Donor	Donor:PCBM ratio	As cast[a]	Annealed[b]	As cast[a]	Annealed[b]	As cast[a]	Annealed[b]	As cast[a]	Annealed[b]
BDT	1:3	0.19	0.49	2.79	3.70	28.1	29.9	0.15	0.54
	1:4	0.39	0.51	4.44	4.10	31.0	32.8	0.53	0.68
	1:5	0.47	0.54	4.05	3.18	29.4	30.6	0.56	0.52
BT	1:3	0.04	0.07	1.64	1.68	25.0	25.3	0.018	0.031
	1:4	0.26	0.44	2.35	3.20	27.7	29.8	0.17	0.42
	1:5	0.46	0.49	3.21	3.28	29.7	30.8	0.44	0.49

[a]Devices without annealing. [b]Devices annealed at 80 °C for 20 min.

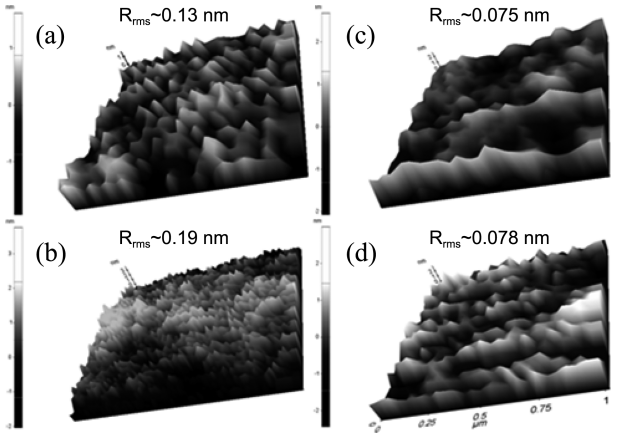

Figure 5. AFM images of as cast (a, b) and annealed (c, d) **BDT**/PCBM = 1:3 blended solid film (a, c) and **BDT**/PCBM = 1:4 blended solid film (b, d).

the **BT**/PCBM = 1:4 blended film (0.20 nm) and **BT**/PCBM = 1:5 blended film (0.28 nm) were slightly higher than those of the **BDT**-containing blended films due to the more efficient self-aggregation of the **BT** molecules. A molecule containing one TPA unit (**BT**) has a flatter surface than a molecule containing two TPA units (**BDT**). Interestingly, the rms roughnesses of the annealed devices were 0.075 nm, 0.078 nm, 0.087 nm, and 0.21 nm in the cases of **BDT**/PCBM = 1:3, **BDT**/PCBM = 1:4, **BT**/PCBM = 1:4, and **BT**/PCBM = 1:5, respectively. The effect of the increased PCBM ratio on the rms roughnesses of the **BDT** and **BT films** blended with PCBM is not presently clear. The smooth film morphology helps increase the PCE because of the suppressed phase separation of the donor and acceptor and helps improves the contact with the active layer and Al electrode.[15] Assuming that the donor-donor or acceptor-acceptor interactions are intrinsically stronger than the donor-acceptor interactions, severe phase separation results. For all the annealed devices, the AFM images reveal a very small degree of phase separation (Fig. 5 and S3†), indicating that the donor-acceptor interactions were more favorable than the donor-donor or acceptor-acceptor interactions. The surface roughness of the film slightly decreased in the case of the annealed devices. Thus, we could state that thermal annealing helped in preventing phase separation.

Conclusion

We developed new solution-processable donor materials, **BDT** and **BT**, which consist of thiazole and triphenylamine units linked by conjugated bonds. BHJ devices were fabricated by spin coating a blended solution of **BDT** or **BT** and PCBM at different weight ratios (1:3, 1:4, 1:5, w/w). We confirmed that the film morphology and PCE were better in the case of annealed devices than in the case of non-annealed devices. Optimum device performance was observed for the annealed device with a **BDT**/PCBM ratio of 1:4; the maximum open-circuit voltage, short-circuit current, and PCE of this device were 0.51 V, 4.10 mA cm^{-2}, and 0.68%, respectively, under simulated AM 1.5 solar irradiation (100 mW cm^{-2}). Our results show that thiazole derivatives are promising donor materials for BHJ solar cells.

Acknowledgments. This study was supported by a grant from the Basic Science Research Program through the National Research Foundation of Korea (NRF) funded by the Ministry of Education, Science and Technology (MEST) of Korea for the Center for Next Generation Dye-sensitized Solar Cells (No. 2012-0000591), and by the New & Renewable Energy Technology Development Program of the KETEP grant (No. 20113020010070) funded by the Ministry of Knowledge Economy.

References

1. Kim, J. Y.; Lee, K.; Coates, N. E.; Moses, D.; Nguyen, T.-Q.; Dante, M.; Heeger, A. J. *Science* **2007**, *317*, 222.
2. Dennler, G.; Scharber, M. C.; Brabec, C. J. *Adv. Mater.* **2009**, *21*, 1323.
3. (a) Ma, W.; Yang, C.; Gong, X.; Lee K.; Heeger, A. J. *Adv. Funct. Mater.* **2005**, *15*, 1617. (b) Thompson, B. C.; Frechet, J. M. J. *Angew. Chem. Int. Ed.* **2008**, *47*, 58. (c) Hoppe, H.; Sariciftci, N. S. *J. Mater. Chem.* **2006**, *16*, 45.
4. (a) Roquet, S.; Bettignies, R. D.; Leriche, P.; Cravino, A.; Roncali, J. *J. Mater. Chem.* **2006**, *16*, 3040. (b) Karpe, S.; Cravino, A.; Frère, P.; Allain, M.; Mabon, G.; Roncali, J. *Adv. Funct. Mater.* **2007**, *17*, 1163. (c) Liu, Y.; Wan, X.; Yin, B.; Zhou, J.; Long, G.; Yin, S.; Chen, Y. *J. Mater. Chem.* **2010**, *20*, 2464.
5. (a) Shirota, Y. *J. Mater. Chem.* **2000**, *10*, 1. (b) Shirota, Y. *J. Mater. Chem.* **2005**, *15*, 75. (c) Noda, T.; Ogawa, H.; Noma, N.; Shirota, Y. *Adv. Mater.* **1997**, *9*, 720. (d) Kageyama, H.; Ohishi, H.; Tanaka, M.; Ohmori, Y.; Shirota, Y. *Adv. Funct. Mater.* **2009**,

19, 3948.
6. (a) Roncali, J. *Acc. Chem. Res*. **2009**, *42*, 1719. (b) Roquet, S.; Cravino, A.; Leriche, P.; Alévêque, O.; Frère, P.; Roncali, J. *J. Am. Chem. Soc.* **2006**, *128*, 3459. (c) Cravino, A.; Roquet, S.; Leriche, P.; Alévêque, O.; Frère, P.; Roncali, J. *Chem. Commun.* **2006**, 1416.
7. (a) He, C.; He, Q.; Yang, X.; Wu, G.; Yang, C.; Bai, F.; Shuai, Z.; Wang, L.; Li, Y. *J. Phys. Chem. C*. **2007**, *111*, 8661. (b) Li, K.; Qu, J.; Xu, B.; Zhou, Y.; Liu, L.; Peng, P.; Tian, W. *New J. Chem.* **2009**, *33*, 2120.
8. (a) Huo, L.; He, C.; Han, M.; Zhou, E.; Li, Y. *J. Polym. Sci. Pol. Chem.* **2007**, *45*, 3861. (b) He, Q.; He, C.; Sun, Y.; Wu, H.; Li, Y.; Bai, F. *Thin Solid Films* **2008**, *516*, 5935. (c) He, C.; He, Q.; Yi, Y.; Wu, G.; Bai, F.; Shuai, Z.; Li, Y. *J. Mater. Chem.* **2008**, *18*, 4085. (d) Zhang, J.; Yang, Y.; He, C.; He, Y.; Zhao, G.; Li, Y. *Macromolecules* **2009**, *42*, 7619. (e) Shang, H.; Fan, H.; Shi, Q.; Li, S.; Li, Y.; Zhan, X. *Sol. Energy Mater. Sol. Cells* **2007**, *94*, 457. (f) Yang, Y.; Zhang, J.; Zhou, Y.; Zhao, G.; He, C.; Li, Y.; Anderson, M.; Inganäs, O.; Zhang, F. *J. Phys. Chem. C* **2010**, *114*, 3701.
9. (a) Biniek, L.; Chochos, C. L.; Leclerc, N.; Hadziioannou, G.; Kallitsis, J. K.; Bechara, R.; Lévêque, P.; Heiser, T. *J. Mater. Chem.* **2009**, *19*, 4946. (b) Mei, J.; Heston, N. C.; Vasilyeva, S. V.; Reynolds, J. R. *Macromolecules* **2009**, *42*, 1482. (c) Li, W.; Du, C.; Li, F.; Zhou, Y.; Fahlman, M.; Bo, Z.; Zhang, F. *Chem. Mater.* **2009**, *21*, 5327. (d) Mikroyannidis, J. A.; Suresh, P.; Sharma, G. D. *Org. Electron.* **2010**, *11*, 311.
10. (a) Campos, L. M.; Tontcheva, A.; Günes, S.; Sonmez, G.; Neugebauer, H.; Sariciftci, N. S.; Wudl, F. *Chem. Mater.* **2005**, *17*, 4031. (b) Zhang, F.; Perzon, E.; Wang, X.; Mammo, W.; Anderson, M. R.; Inganäs, O. *Adv. Funct. Mater.* **2005**, *15*, 745. (c) Zoombelt, A. P.; Fonrodona, M.; Turbiez, M. G. R.; Wienk, M. M.; Janssen, R. A. J. *J. Mater. Chem.* **2009**, *19*, 5336.
11. (a) Sharma, G. D.; Roy, M. S.; Sangodkar, G. S.; Gupta, S. K. *Synthetic Matals* **1996**, *83*, 1. (b) Roy, M. S.; Sharma, G. D.; Gupta, S. K. *Thin Solid Films* **1997**, *310*, 279. (c) Sharma, G. D.; Choudhary, V. S.; Roy, M. S. *Sol. Energy Mater. Sol. Cells* **2007**, *91*, 275. (d) Suresh, P.; Sharma, S. K.; Roy, M. S.; Sharma, G. D. *Synthetic Metals* **2009**, *159*, 52. (e) Jung, I. H.; Yu, J.; Jeong, E.; Kim, J.; Kwon, S.; Kong, H.; Lee, K.; Woo, H. Y.; Shim, H.-K. *Chem. Eur. J.* **2010**, *16*, 3743.
12. Kwon, J.; Lee, W.; Kim, J.-Y.; Noh, S.; Lee, C.; Hong, J.-I. *New J. Chem.* **2010**, *34*, 744.
13. Hassan, J.; Lavenot, L.; Gozzi, C.; Lemaire, M. *Tetrahedron Lett.* **1999**, *40*, 857.
14. Sariciftci, N. S.; Smilowitz, L.; Heeger, A. J.; Wudl, F. *Science* **1992**, *258*, 1474.
15. Sun, X.; Zhou, Y.; Wu, W.; Liu, Y.; Tian, W.; Yu, G.; Qiu, W.; Chen, S.; Zhu, D. *J. Phys. Chem. B* **2006**, *110*, 7702.
16. Tamayo, A.; Kent, T.; Tantitiwat, M.; Dante, M. A.; Rogers, J.; Nguyen, T.-Q. *Energy Environ. Sci.* **2009**, *2*, 1180.